Ultralow-frequency modulation of whistler-mode wave growth

C. E. J. Watt,[1] A. W. Degeling,[1] R. Rankin,[1] K. R. Murphy,[1] I. J. Rae,[1] and H. J. Singer[2]

[1]   Measurements from ground-based magnetometers and riometers at auroral latitudes have demonstrated that energetic (~30–300 keV) electron precipitation can be modulated in the presence of magnetic field oscillations at ultralow frequencies. It has previously been proposed that an ultralow-frequency (ULF) wave would modulate field and plasma properties near the equatorial plane, thus modifying the growth rates of whistler-mode waves. In turn, the resulting whistler-mode waves would mediate the pitch angle scattering of electrons resulting in ionospheric precipitation. In this paper, we investigate this hypothesis by quantifying the changes to the linear growth rate expected due to a slow change in the local magnetic field strength for parameters typical of the equatorial region around $6.6 R_E$ radial distance. To constrain our study, we determine the largest possible ULF wave amplitudes from measurements of the magnetic field at geosynchronous orbit. Using nearly ten years of observations from two satellites, we demonstrate that the variation in magnetic field strength due to oscillations at 2 mHz does not exceed ±10% of the background field. Modifications to the plasma density and temperature anisotropy are estimated using idealized models. For low temperature anisotropy, there is little change in the whistler-mode growth rates even for the largest ULF wave amplitude. Only for large temperature anisotropies can whistler-mode growth rates be modulated sufficiently to account for the changes in electron precipitation measured by riometers at auroral latitudes.

1.   Introduction

[2]   The co-location of ground-based magnetometers and riometers at auroral latitudes has firmly established that concurrent, periodic variations in the signals of each instrument can occur at ultralow frequencies (f < 30Hz) [*Ziauddin*, 1960; *Anger et al.*, 1963; *Brown*, 1964; *Parthasarathy and Hessler*, 1964; *Hargreaves*, 1969; *Yuan and Jacka*, 1969; *Hunsucker et al.*, 1972; *Berkey*, 1974; *Brown*, 1975; *Heacock and Hunsucker*, 1977; *Olson et al.*, 1980; *Paquette et al.*, 1994; *Posch et al.*, 1999; *Spanswick et al.*, 2005; *Rae et al.*, 2007; *Roldugin and Roldugin*, 2008]. Ground-based magnetometers measure the superposition of the Earth's magnetic field and much smaller contributions from nearby overhead ionospheric current systems, allowing researchers to deduce the presence of large-scale oscillations in the magnetosphere. Riometers measure the absorption of cosmic radio noise in the D-region (60–90 km altitude) of the ionosphere. Variations in cosmic noise absorption (CNA) beyond the usual diurnal variation can be attributed to increased ionization in the D-region, and imply the presence of increased electron precipitation in the energy range 30 keV to a few hundred keV. Co-located instruments at auroral latitudes show contemporary modulation of riometer and magnetometer signals at frequencies of a few mHz [*Ziauddin*, 1960; *Anger et al.*, 1963; *Rae et al.*, 2007; *Roldugin and Roldugin*, 2008]. Modulation of both signals is also observed at higher frequencies of a few tens of mHz [*Yuan and Jacka*, 1969] and up to 0.2Hz [*Heacock and Hunsucker*, 1977]. Riometer pulsations are often confined to narrow bands in latitude 1–2° wide [*Parthasarathy and Hessler*, 1964] but can be much more extended in longitude [*Hargreaves*, 1969]. The periodic modulation of cosmic noise absorption is predominately observed in the morning sector [*Brown*, 1964, 1975; *Paquette et al.*, 1994; *Spanswick et al.*, 2005]. Observations of multiple events reveal that there is a phase motion of both riometer and magnetometer signals away from noon [*Olson et al.*, 1980]. Precipitation pulsations mainly occur on an already enhanced background precipitation [*Spanswick et al.*, 2005]. Most importantly, observations indicate that while all riometer pulsations are accompanied by magnetometer pulsations at similar frequencies, magnetometer pulsations can exist without concurrent riometer fluctuations [*Olson et al.*, 1980; *Spanswick et al.*, 2005]. However, the relationship between the onset of magnetic pulsations and the onset of riometer pulsations is not as simple [*Paquette et al.*, 1994].

[3]   Energetic electron precipitation can also be inferred from X-ray aurora emissions [e.g., *Omholt*, 1971]. Similar

[1]Department of Physics, University of Alberta, Edmonton, Alberta, Canada.
[2]NOAA Space Environment Center, Boulder, Colorado, USA.

relationships between X-ray and magnetometer pulsations are found, mainly on the dayside of the magnetosphere and at auroral latitudes [*Ullaland et al.*, 1967; *McPherron et al.*, 1968; *Arthur et al.*, 1979; *Asnes et al.*, 2004].

[4] The comprehensive statistical results of *Spanswick et al.* [2005] suggest that necessary requirements for the modulation of energetic particle precipitation are a magnetic pulsation and increased energetic electron flux in the magnetosphere. It is therefore logical to suggest that the magnetic pulsation is responsible for the modulation in energetic particle precipitation rather than the other way round. *Coroniti and Kennel* [1970] suggest that the magnetic ULF wave could be responsible for the modulation of the energetic particles through a wave-wave interaction in the magnetosphere. Pitch angle diffusion due to very low frequency (VLF) whistler-mode waves in the magnetosphere can be responsible for the loss of charged particles to the ionosphere and atmosphere [*Kennel and Petschek*, 1966]. Since one of the actions of the magnetic ULF wave is to modulate the total magnetic field strength, it follows that the growth-rates of whistler-mode waves, which depend upon the local electron gyrofrequency $\Omega_e = q_e B/m_e$, would be affected (q_e and m_e are the electron charge and mass, respectively, and B is the ambient magnetic field strength). The equatorial electron distribution function may also be altered by the slowly varying ULF magnetic field. *Coroniti and Kennel* [1970] argue that these slow changes would modulate the growth rates of whistler-mode waves, which would in turn modulate the pitch angle diffusion in the magnetosphere, and therefore the rate of particle precipitation, yielding the observed modulation of riometer signals and X-ray aurora emissions.

[5] Observational support of *Coroniti and Kennel*' [1970] model (which we will refer to as the C-K model) demonstrates the modulation of VLF wave power at ULF periods both in situ [*Glassmeier et al.*, 1988] and on the ground [*Morrison*, 1990; *Smith et al.*, 1998; *Singh et al.*, 2005; *Manninen et al.*, 2010].

[6] The theory of whistler-mode wave generation has moved on considerably since the time of the C-K model. A nonlinear analysis of whistler-mode wave generation in the inhomogeneous magnetosphere shows that although the initial growth of whistler-mode waves is linear, once an amplitude threshold is reached, the nonlinear wave growth is faster than the linear theory predicts [*Omura et al.*, 2008, 2009]. This nonlinear theory reproduces the rising frequency emissions characteristic of whistler-mode chorus, and can explain the observed absence of whistler-mode waves at frequencies of half the gyrofrequency [e.g., *Tsurutani and Smith*, 1974]. However, this new theory [*Omura et al.*, 2008, 2009], reinforced by full particle and hybrid simulations [*Katoh and Omura*, 2007; *Hikishima et al.*, 2009a, 2009b, 2010; *Katoh and Omura*, 2011], concentrates only on waves with parallel wave vectors, and by necessity, describes only very short timescales in the plasma evolution. In this study, we extend the analysis to consider waves with oblique wave vectors, but limit our study to linear theory. By estimating realistic changes in magnetospheric plasma and magnetic field strength during ULF wave oscillations, we aim to show how much, or how little, instability conditions in the magnetosphere can change due to ULF wave oscillations. The results presented in this paper will inform future work on the complex problem of the modulation of energetic particle precipitation by ULF waves.

[7] In this paper, we investigate the changes in local whistler-mode growth rates due to slow variations in the ambient magnetic field, cold plasma density, and hot plasma distribution function due to a large-scale ultralow-frequency wave. We present the dispersion relation for whistler-mode waves in Section 2 and the magnetospheric plasma model in Section 5, where we discuss which plasma variables will be affected by the slow action of the ULF wave. Section 3 presents the effects on the whistler-mode growth rates of changes in each of these plasma variables in turn. Section 4 describes the data sets and models used to estimate the possible changes in field and plasma properties possible due to a large-amplitude ULF wave oscillation. Observations from the Geostationary Operational Environmental Satellite (GOES) system [*Singer et al.*, 1996] are used to determine the changes in magnetic field strength possible due to ULF wave activity at geosynchronous orbit (~$6.6R_E$ radial distance). An ideal magnetohydrodynamic (MHD) model of ULF waves [*Degeling et al.*, 2008] is used to estimate the changes in cold plasma density possible at the equatorial plane of an idealized dipolar magnetosphere as a result of the largest ULF wave amplitudes observed by GOES. Finally, we estimate the changes in the local distribution function which would result from the magnetic field compressions and rarefactions. The full warm plasma dispersion relation is used in section 6 to estimate the changes in growth rates due to the waves. We discuss these results in Section 7 and present our conclusions in the final section.

2. Dispersion Relation

[8] Whistler-mode waves can be driven unstable by a temperature anisotropy [e.g., *Gary*, 1993] or a high-energy beam [e.g., *Sauer and Sydora*, 2010]. We focus in this work on the temperature anisotropy whistler-mode instability which is believed to operate near the equator in the magnetosphere [e.g., *Kennel and Petschek*, 1966; *Coroniti and Kennel*, 1970; *Anderson and Maeda*, 1977; *MacDonald et al.*, 2008; *Summers et al.*, 2009] and we will include both field-aligned and oblique wave vectors in our analysis.

[9] We characterize the plasma as mostly cold, with a small warm electron component which causes the whistler-mode instability. We assume that the spatial inhomogeneities of the plasma have length-scales large enough that the plasma and magnetic field may be considered to be locally uniform. The real frequency ω_r of the whistler-mode waves will be determined by solutions to the cold plasma dispersion relation

$$D \equiv A_S \mu^4 + B_S \mu^2 + C_S = 0 \qquad (1)$$

where μ is the refractive index, and A_S, B_S and C_S are the cold plasma parameters as given by *Stix* [1992, pp. 8–9]. If we also assume that the imaginary part of the frequency (the growth/damping rate) $\omega_i \ll \omega_r$ then we can use the imaginary part of a hot plasma dispersion relation D_H to calculate ω_i [e.g., *Xiao et al.*, 1998; *Sazhin*, 1991],

$$\omega_i = -\frac{\Im D_H}{(\partial[\Re D]/\partial\omega_r)} \qquad (2)$$

where

$$D_H = A_H \mu^4 + B_H \mu^2 + C_H, \qquad (3)$$

and A_H, B_H and C_H are the equivalent of A_S, B_S and C_S in a warm plasma [*Sazhin*, 1991; *Summers et al.*, 1994]:

$$A_H = K_{xx} \sin^2 \psi + 2K_{xz} \sin \psi \cos \psi + K_{zz} \cos^2 \psi, \qquad (4)$$

$$B_H = K_{xz}^2 - K_{xx}K_{zz} - A_H K_{yy} - \left(K_{xy} \sin \psi - K_{yz} \cos \psi\right)^2, \qquad (5)$$

$$C_H = K_{yy}\left(K_{xx}K_{zz} - K_{xz}^2\right) + K_{xy}\left(K_{xy}K_{zz} + 2K_{yz}K_{xz}\right) + K_{xx}K_{yz}^2. \qquad (6)$$

Here, ψ is the angle between the wave vector and the magnetic field, and the K_{ij} are the nine elements of the dielectric tensor K which can be calculated once a suitable form for the unstable electron distribution function has been supplied. We assume that the distribution function is even in parallel velocity $v_\parallel$ so that $K_{zx} = K_{xz}$, $K_{zy} = -K_{yz}$ and $K_{yx} = -K_{xy}$.

[10] Observations in the plasma sheet indicate that the Lorentzian distribution function with $\kappa < 7$ is an accurate description of the warm electron population [*Christon et al.*, 1988; *Kletzing et al.*, 2003]; therefore, we model the warm plasma component $f_{e,0}$ at the magnetic equator using a generalized Lorentzian form [e.g., *Summers and Thorne*, 1991]:

$$f_{e,0}\left(v_\parallel, v_\perp\right) = \frac{\nu n}{\pi^{3/2}\theta_\perp^2 \theta_\parallel \kappa^{3/2}} \frac{\Gamma(\kappa+1)}{\Gamma(\kappa-1/2)} \left(1 + \frac{v_\parallel^2}{\kappa\theta_\parallel^2} + \frac{v_\perp^2}{\kappa\theta_\perp^2}\right)^{-(\kappa+1)}, \qquad (7)$$

where $v_\parallel$, $v_\perp$ are velocities parallel and perpendicular to the magnetic field B, $\nu \ll 1$ is the ratio of the number density of the sparse warm component to the cold dense component, κ is the spectral index, Γ is the standard gamma function, and the thermal speeds parallel and perpendicular to the field are given by

$$\theta_{\parallel,\perp} = \left(\frac{2\kappa - 3}{\kappa}\right)^{1/2} \left(\frac{T_{\parallel,\perp}}{m_e}\right)^{1/2}. \qquad (8)$$

The parallel and perpendicular temperatures of the warm plasma component are denoted $T_\parallel$, $T_\perp$. The change in magnetic field strength due to the ULF oscillation is very slow compared to the growth time of the VLF waves, so we assume that the whistler-mode growth is part of a steady state process where wave growth is balanced by pitch angle scattering. This situation can only be accomplished in regions where there is a steady source of particles which maintains the temperature anisotropy above the threshold for the whistler-mode instability [*Kennel and Petschek*, 1966; *Coroniti and Kennel*, 1970]. Hence we choose a distribution function without any loss cone features so that we may include both the trapped and precipitating electrons. It would be reasonable to assume that the level of electron temperature anisotropy maintained by this pitch angle scattering process depends on the details of the source population of electrons, and so one of the free parameters in our model will be the temperature anisotropy $A = (\theta_\perp^2/\theta_\parallel^2) - 1$.

[11] *Summers et al.* [1994] present non-relativistic expressions for the K_{ij} in equations (4)–(6). These expres-

sions involve the modified plasma dispersion function Z^* [*Summers and Thorne*, 1991] and are evaluated numerically to give the imaginary part of D_H without any further assumptions (see Appendix A). The function Z^* is limited to integer [*Summers and Thorne*, 1991] and half-integer [*Summers et al.*, 1996] values of κ, but will suffice for the demonstration in this paper (a more generalized plasma dispersion function for Lorentzian plasma for all values of κ can be found in work by *Hellberg and Mace* [2002] and *Mace and Hellberg* [2009]). The aim of this paper is to study growth of whistler-mode waves over a region of the magnetosphere where it is inappropriate to further simplify the warm plasma dispersion relation assuming that the plasma frequency is much larger than the gyrofrequency [cf. *Kennel and Petschek*, 1966; *Brinca*, 1972] or to confine the analysis to parallel wave vectors [*Xiao et al.*, 1998; *Summers et al.*, 2009; *Mace and Sydora*, 2010]. We will, however, restrict our analysis to modest temperatures ($T_e \leq 25$ keV) such that the errors introduced by the non-relativistic dielectric tensor are minimized [see *Xiao et al.*, 1998]. The derivation of a warm dielectric tensor for oblique waves in a relativistic plasma with a high-energy tail is a formidable challenge, and will be attempted in future work.

[12] The values of the growth rates obtained by equation (2) for parallel wave vectors compare favorably with the results presented by *Xiao et al.* [1998], where a similar plasma model comprising a dominant cold electron population and a tenuous warm unstable electron component is used. *Mace and Sydora* [2010] present results from an analysis where the whole electron population is described using a warm Lorentzian distribution function. The behavior of the growth rates for parallel wave vectors obtained from the equations above compares favorably with the results presented by *Mace and Sydora* [2010] for integer values of κ, although the magnitudes are slightly different. We are therefore confident that our numerical evaluation of the warm plasma dielectric tensor [*Summers et al.*, 1994] and subsequent evaluation of the growth rates using equation (2) is robust.

3. Whistler-Mode Wave Growth Rates

[13] Observations of the ULF modulation of riometer and magnetometer signals tend to occur at auroral latitudes in the morning sector [e.g., *Spanswick et al.*, 2005]. Mapping of these ground-stations along the magnetic field into the magnetosphere is not straightforward, but we estimate that these measurements correspond to a region which is between $6R_E$ and $9R_E$ radial distance in the equatorial plane.

[14] The parameters considered in this section are chosen to be indicative of possible conditions at geosynchronous orbit ($6.6R_E$ radial distance), although the local number density and temperature can vary according to local time and magnetospheric activity [e.g., *Denton et al.*, 2005]. We choose the geosynchronous orbit distance as it is here where possibly the most information has been gained about the local plasma conditions and ULF magnetic field oscillations. However, values of A, ω_{pe}/Ω_e and $T_{\parallel,e}$ are similar for a range of radial distances $6R_E < r < 9R_E$, so the results presented in this section should be applicable over a wider region in the magnetosphere.

[15] Throughout this paper, we choose a ratio of hot electrons to cold electrons which is a small fraction $\nu = 0.01$.
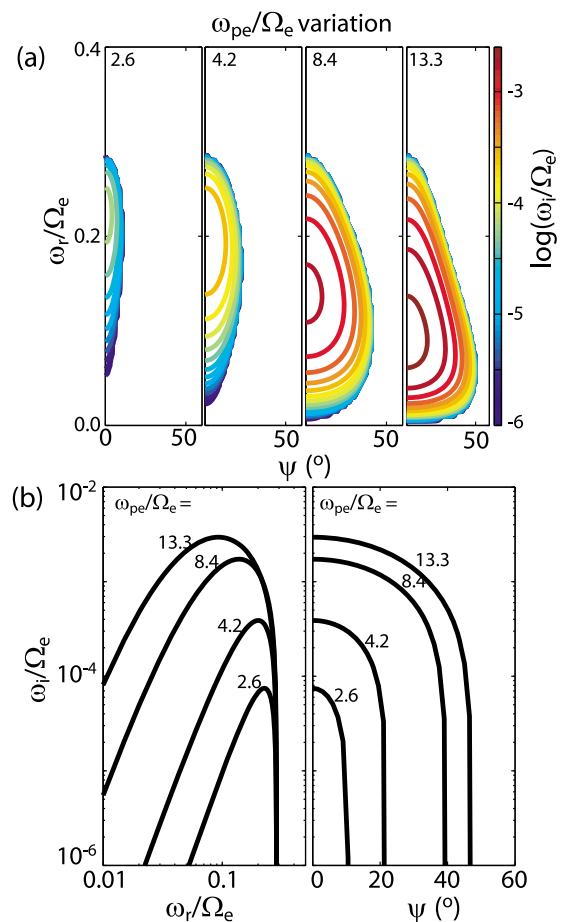
Anisotropy variation
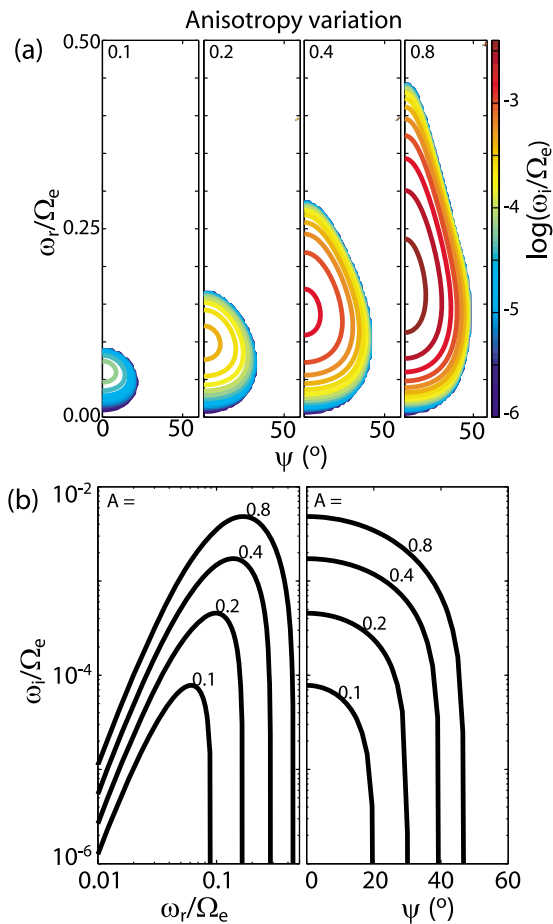
Figure 1. (a) Normalized solutions ω_i/Ω_e of the warm plasma dispersion relation as a function of wavenormal angle ψ and normalized real frequency ω_r/Ω_e for four cases with constant magnetic field strength, parallel temperature and number density, but different temperature anisotropy. White areas indicate damped waves. (b) Slices through the contour plots in Figure 1a (left) for $\psi = 0$ and (right) for the frequency of maximum growth.

This ratio can vary significantly at geosynchronous radial distance; it can be very small when there is a significant cold electron population due to e.g. plasmaspheric plumes, or it can be very large following an injection of hot plasma from the plasma sheet. Note that in the original model of *Coroniti and Kennel* [1970], it is assumed that ν is small. Large values of ν should be investigated using full solutions to the plasma dispersion relation, but to make appropriate comparisons with previous work, we will restrict our analysis to the simpler case where the cold plasma provides the real part of the frequency and the warm plasma provides the imaginary part. We will investigate the modification to whistler-mode growth rates in a hot electron-dominated plasma in future work.

[16] Figure 1 shows the growth rates given by equation (2) for $B = 108$ nT, $n_e = 8.0 \times 10^6$ m^{-3}, $T_{\|,e} = 15$ keV and temperature anisotropies varying between $A = 0.1$ and $A = 0.8$. For these parameters, $\omega_{pe}/\Omega_e = 8.4$. Figure 1a shows that the maximum growth rate increases by almost two orders of magnitude as the temperature anisotropy is increased from

0.1 to 0.8. The maximum growth rate always occurs for parallel propagation. The real frequency at which the maximum growth rate occurs also increases as A is increased, from $0.06\Omega_e$ to $0.16\Omega_e$. Figure 1b demonstrates that the range of growing waves increases with increasing temperature anisotropy, in both frequency and wavenormal angle ψ relative to the ambient magnetic field. However, growth rates more than 10% of the maximum growth rate are confined to $|\psi| < 40°$ even for the case $A = 0.8$.

[17] Figure 2 demonstrates the variation of the growth rates when the parameter ω_{pe}/Ω_e is varied. We accomplish this by keeping $B = 108$ nT, $T_{\|,e} = 15$ keV and $A = 0.4$ fixed, and varying the electron number density for four different cases $n_e = 8.0 \times 10^5$, 2.0×10^6, 8.0×10^6, and 2.0×10^7 m^{-3}; ω_{pe}/Ω_e varies between 2.6 and 13.3 as a result. These number densities likely span a larger range than that expected at geosynchronous orbit, but serve to demonstrate how ω_i varies with ω_{pe}/Ω_e (remember that this parameter

ω_{pe}/Ω_e variation

Figure 2. (a) Normalized solutions ω_i/Ω_e of the warm plasma dispersion relation as a function of wavenormal angle ψ and normalized real frequency ω_r/Ω_e for four cases with constant magnetic field strength, parallel temperature and temperature anisotropy, but different values of ω_{pe}/Ω_e (controlled by varying the number density). White areas indicate damped waves. (b) Slices through the contour plots in Figure 2a (left) for $\psi = 0$ and (right) for the frequency of maximum growth.
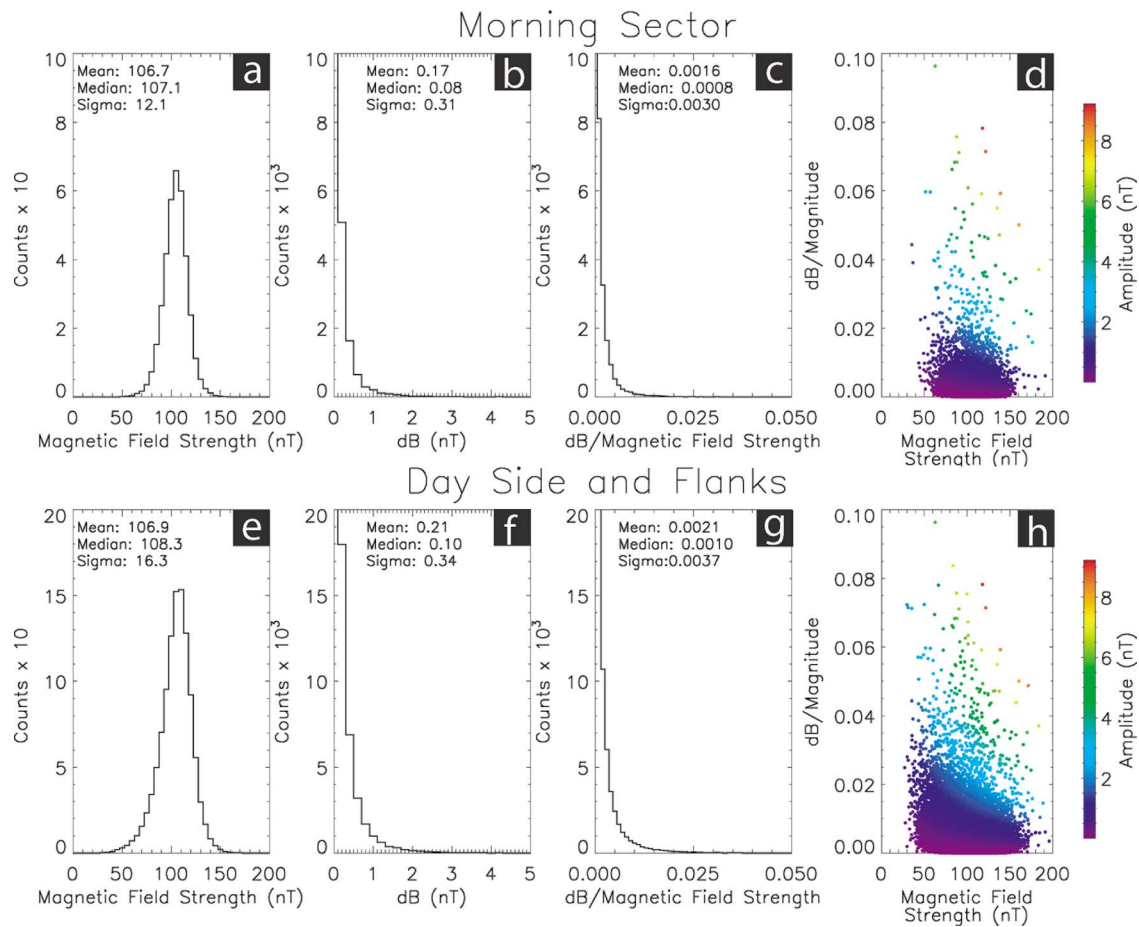
Figure 3. Statistical survey of GOES East and West magnetic field perturbation data from 1 December 1995 to 6 May 2005: occurrence distributions of (a, e) magnetic field strength, (b, f) compressional magnetic field perturbations, and (c, g) normalized compressional magnetic field perturbations, with (d, h) a scatterplot of the compressional perturbation as a function of magnetic field strength and normalized perturbation for (Figures 3a–3d) 3–9 MLT and (Figures 3e–3h) 3–21 MLT.

will also vary due to variations in the ambient magnetic field strength). Figure 2 shows that the growth rates and range of unstable ψ increase as ω_{pe}/Ω_e increases, similarly to the anisotropy variation. On the other hand, the range of unstable frequencies remains constant, and the real frequency for which growth is maximized decreases as ω_{pe}/Ω_e is increased. Growth rates more than 10% of the maximum growth rate are confined to $|\psi| < 40°$ even for the case with the largest number density.

[18] *Xiao et al.* [1998] show that for parallel wave vectors, the size of the growth rates of whistler-mode waves is directly proportional to the ratio of the hot to cold electron number density ν. This is also true for oblique modes, so we do not show those results graphically. The parameter ν does not alter the range of unstable frequencies or wave vectors, nor does it change the real frequency for which growth is maximized.

[19] Figures 1 and 2 indicate that for most reasonable values of the electron number density and temperature anisotropy (see, e.g., *MacDonald et al.* [2008], who indicate that $A < 1$ and $n_e \sim 1.0 \times 10^6$ m^{-3}, implying $\omega_{pe}/\Omega_e \sim 3$), whistler-mode waves will mostly be excited with wave-

normal angles <45°, and growth rates which peak for real frequencies $\omega_r \sim 0.2\Omega_e$.

4. ULF Wave Oscillations at Geosynchronous Orbit

[20] Before we may estimate the change in the plasma parameters due to the slow magnetic field perturbation, we must first predict the possible size of this perturbation. *Spanswick et al.* [2005] focus on riometer oscillations in the Pc5 range of frequencies (1.67–6.67 mHz). Median compressional ULF wave power at geosynchronous orbit over 1.0–8.3 mHz decreases with frequency [*Huang et al.*, 2010], so for this demonstration, we choose a representative ULF wave frequency of ~2 mHz, which is near the lower end of the Pc5 range. This frequency is therefore more likely to correspond to some of the largest amplitude compressional waves observed at geosynchronous orbit.

[21] Figure 3 shows a statistical analysis of the magnetic field strength and variations in magnetic field strength at 1.94 mHz at geosynchronous orbit as measured by both the GOES East and West satellites [*Singer et al.*, 1996] between
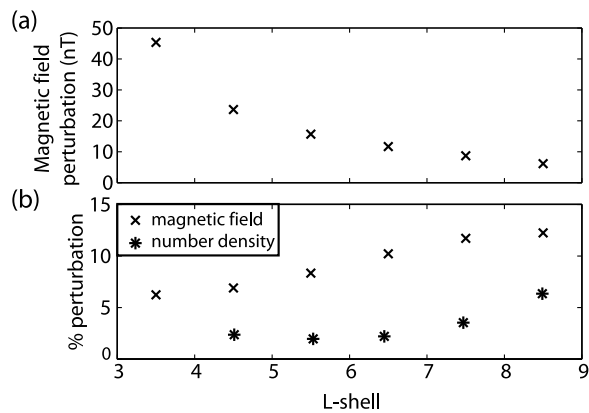
Figure 4. (a) Magnitude of magnetic field strength perturbation at the magnetic equator predicted by an ideal MHD model of a $m = 0$ global compressional ULF wave with $f = 2$ mHz. (b) Perturbation of magnetic field strength (crosses) and cold plasma number density (asterisks) as a percentage of their unperturbed values.

1 December 1995 and 6 May 2005. The magnetometer observations are transformed from the geocentric solar magnetospheric (GSM) coordinate system to a field-aligned coordinate (FAC) system, and then divided into 24 hourly segments starting at midnight universal time (UT). We remove all hourly segments when the GOES satellites are located within $1.5R_E$ of the theoretical magnetopause. There are periods of extreme magnetospheric compression where the GOES satellites can leave the magnetosphere and sample the magnetosheath; these periods are removed so that we may focus solely on magnetospheric compressional wave amplitudes. Similarly, any hourly time series containing a data gap or data spike is excluded. The compressional magnetic field variations are then determined by applying a Hanning window to each hourly segment, before taking the Fourier transform. We define the amplitude of the compressional wave dB as the amplitude of the field-aligned magnetic field component at 1.94 mHz, and the magnetic field strength is determined using the median magnetic field strength during each hourly window. *Spanswick et al.* [2005] demonstrate that riometer pulsations are concentrated in the morning sector of the magnetosphere and so we bin our results by magnetic local time (MLT). Results from the morning sector (3–9 MLT) are displayed in Figures 3a–3d, to compare with results from the entire dayside and flank magnetosphere (3–21 MLT) in Figures 3e–3h. Note that perturbations from the night-time sector are excluded from this analysis, since substorm dipolarizations can contribute significant power in low frequencies, and we wish to concentrate on ULF wave oscillations.

[22] Figure 3 shows (Figure 3a) the occurrence distribution of magnetic field strength at $r = 6.6R_E$ in the morning sector, (Figure 3b) the occurrence distribution of compressional wave amplitudes, (Figure 3c) the occurrence distribution of compressional wave amplitudes normalized to the ambient magnetic field strength, and (Figure 3d) a scatterplot of the wave amplitude as a function of magnetic field strength and normalized wave amplitude. 18846 hourly intervals are included in these plots, and the mean, median

and standard deviation values are indicated in Figures 3a–3c. The median compressional wave amplitude is only 0.08 nT, and when expressed as a fraction of the ambient magnetic field strength, the median amplitude is only 0.1%. It is important to remember that these plots contain all oscillations at 1.94 mHz, not just discrete large-amplitude oscillations of the kind invoked by *Coroniti and Kennel* [1970]. We should therefore focus instead on the rarer large amplitude events, which are more likely to correspond to the oscillations required to modulate particle precipitation. Figure 3d shows that no oscillation at 1.94 mHz at $r = 6.6R_E$ exceeds ±10% of the local magnetic field strength. Large amplitude oscillations, as a percentage of the background field, are more likely to occur at low values of magnetic field strength than higher values, but there are no other obvious trends.

[23] Figures 3e–3h show the same information as in Figures 3a–3d but include all intervals binned between 3 and 21MLT. 55770 hourly intervals are included in this larger data set. Even when the whole dayside magnetosphere is included in the analysis, Figure 3h shows that magnetic field oscillations still do not exceed ±10% of the local magnetic field strength.

[24] The observed maximum magnetic field strength oscillation is now used to estimate the possible number density perturbation using an ideal MHD model of ULF waves in a dipolar magnetosphere [*Degeling et al.*, 2008]. For the purposes of this paper, we drive a simple $m = 0$ compressional standing oscillation at 2 mHz from a source located at the outer boundary (magnetopause). The ULF waves form a cavity mode structure between the outer boundary and the MHD fast mode turning point located within the magnetosphere at around $L \sim 4$. The amplitude of these perturbations is scaled such that the magnetic field perturbation at $r = 6.6R_E$ is ±10%, to represent the largest possible wave amplitude observed by the GOES satellites.

[25] The ULF model returns the magnetic field strength at equally spaced points along field lines which are initially dipolar. We interpolate the results onto a grid which is fixed in radial distance and colatitude, and determine the size of the magnetic field perturbations at the magnetic equator as a function of L-shell. The perturbations in Figure 4a represent the largest possible departure from the unperturbed dipolar magnetic field value at the magnetic equator of the model. Figure 4a indicates that the absolute magnitude of the perturbations decreases with radial distance, but Figure 4b (crosses) shows that when expressed as a percentage of the initial local magnetic field strength, the size of the perturbation increases with L-shell.
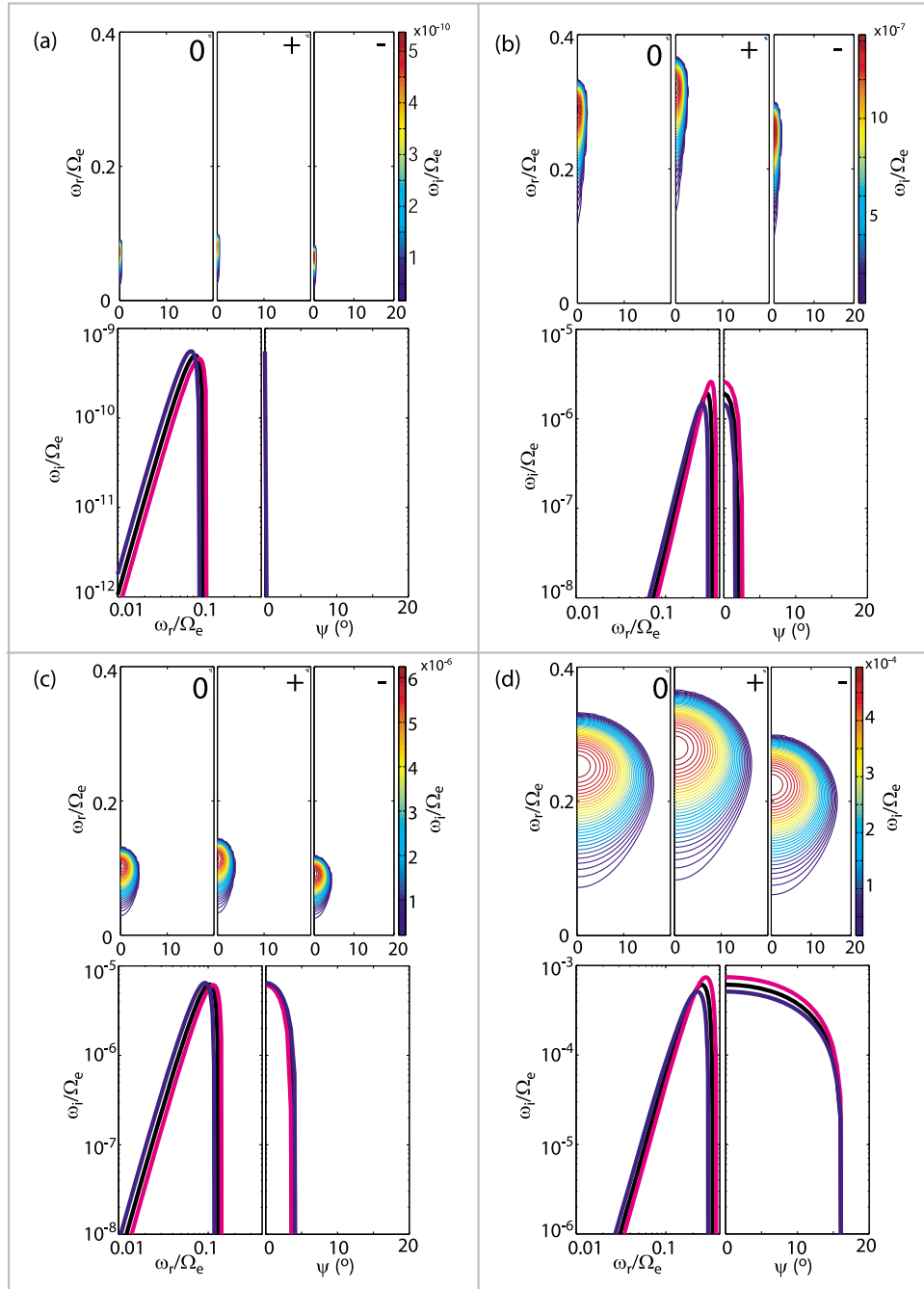
[26] The plasma velocity from the ideal MHD wave model is used to estimate the cold plasma number density variation due to the wave. The continuity equation

$$\frac{\partial \rho_m}{\partial t} + \nabla.(\rho_m \mathbf{v}) = 0 \tag{9}$$

is linearized, providing the estimate

$$\frac{\partial n_1}{\partial t} = \frac{1}{r}\frac{\partial}{\partial r}\left(rn_0 v_{r,1}\right), \tag{10}$$

where $n_{e,0}$ and $n_{e,1}$ are the unperturbed and perturbed parts of the cold plasma number density, and $v_{r,1}$ is the perturbed

Figure 5. Normalized solutions ω_i/Ω_e of the warm plasma dispersion relation in the same format as Figures 1 and 2 for (a) $A = 0.15$, $T_{\|,e} = 1.5$ keV, (b) $A = 0.5$, $T_{\|,e} = 1.5$ keV, (c) $A = 0.15$, $T_{\|,e} = 15$ keV, and (d) $A = 0.5$, $T_{\|,e} = 15$ keV. For the line plots, black indicates solutions for the unperturbed values, magenta indicates solutions when the field is compressed and blue indicates solutions during a rarefaction of the field.

radial plasma velocity. The unperturbed number density is modeled

$$n_0 = 7.5 \times 10^8 \left(\frac{r}{R_0}\right)^{-4}, \quad (11)$$

where $R_0 = 3R_E$. We approximate the time derivative $\partial/\partial t \sim -i\omega_{\mathrm{ULF}}$ where ω_{ULF} is the frequency of the ULF wave. The

resulting expression for the magnitude of the cold number density perturbation is,

$$n_1 = \frac{1}{r\omega_{\mathrm{ULF}}} \frac{\partial}{\partial r}\left(rn_0 v_{r,1}\right), \quad (12)$$

and the estimates from this equation are indicated with asterisks in Figure 4. At radial distances of $r \sim 6.6.R_E$,
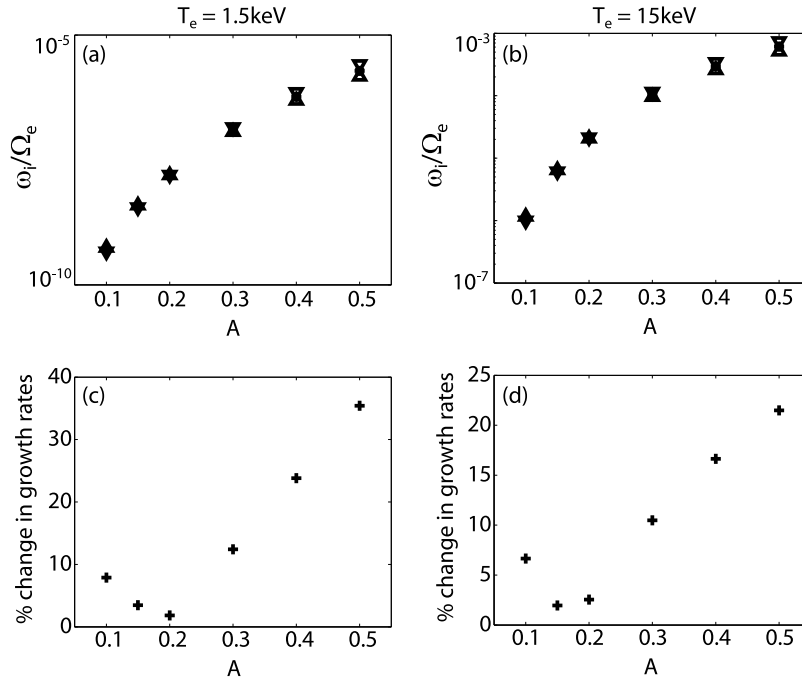
Figure 6. The variation in growth rates as a function of initial temperature anisotropy are shown for (a) $T_{\parallel,e} = 1.5$ keV and (b) $T_{\parallel,e} = 15$ keV. (c, d) The same variations are expressed as a percentage.

given a ±10% variation in magnetic field strength, the cold plasma number density is expected to vary by only ±2%. Under the conditions of ideal MHD, it is expected that the variation of n should be in phase with the variation of B.

5. ULF Variations in the Hot Plasma Component

[27] The gyromotion, bounce motion and drift motion of electrons will be affected by the slowly changing magnetic field. Under the assumption of an axisymmetric magnetosphere and a ULF wave oscillation with no azimuthal component, we will ignore any drift motion effects. Given the assumed presence of pitch angle scattering, it is unlikely that the magnetic moment, or the total kinetic energy, of the particle would be conserved as it bounces from one hemisphere to the other. However, it is expected that an increase in local magnetic field strength, corresponding to a compression of the magnetic field due to the ULF wave, will likely increase the local hot electron number density and increase the average perpendicular energy of the hot population. If one estimates the change in perpendicular electron energy and number density *assuming* that the particle kinetic energy and magnetic moments are constant, then we obtain a prediction which is consistent with above expectations, even though our estimate uses assumptions which contradict the steady state model. In the absence of a much more sophisticated treatment which follows the self-consistent pitch angle scattering over the long period of a ULF wave, we will use these assumptions to estimate general trends in the plasma moments as a result of the slow variation of B. Let $n_H = \nu n_e$, and let a "0" subscript indicate an equilibrium quantity and a "1" subscript indicate a perturbed quantity, to

produce the following expressions for the perturbed hot number density and perpendicular thermal speed [*Xiao and Feng*, 2006],

$$n_{H,1} = \frac{n_{H,0}}{\frac{\theta_\perp^2}{\theta_\parallel^2} + \left(1 - \frac{\theta_\perp^2}{\theta_\parallel^2}\right)\frac{B_0}{B_1}}, \tag{13}$$

$$\theta_{\perp,1}^2 = \frac{\theta_{\perp,0}^2}{\frac{\theta_\perp^2}{\theta_\parallel^2} + \left(1 - \frac{\theta_\perp^2}{\theta_\parallel^2}\right)\frac{B_0}{B_1}}. \tag{14}$$

The long-period ULF wave will therefore likely modulate the temperature anisotropy, the cold electron number density, the hot electron number density and the magnetic field strength. In the following section, we will show how the realistic variation of all four parameters act in concert to change the whistler-mode growth for plasma with different initial temperatures. The analysis above predicts no change in the spectral index κ due to the ULF wave oscillation, and so we fix $\kappa = 4$.

6. ULF Variation of Whistler-Mode Growth Rates

[28] We first investigate four cases, choosing to keep the unperturbed magnetic field strength $B = 108$ nT and unperturbed number density $n_e = 1.0 \times 10^6$ m^{-3} constant among all four cases. These choices result in $\omega_{pe}/\Omega_e = 3.0$. This initial analysis covers combinations of low and high temperature anisotropy ($A = 0.15$ or $A = 0.5$) and low and high parallel electron temperature ($T_{\parallel,e} = 1.5$ keV or $T_{\parallel,e} =$
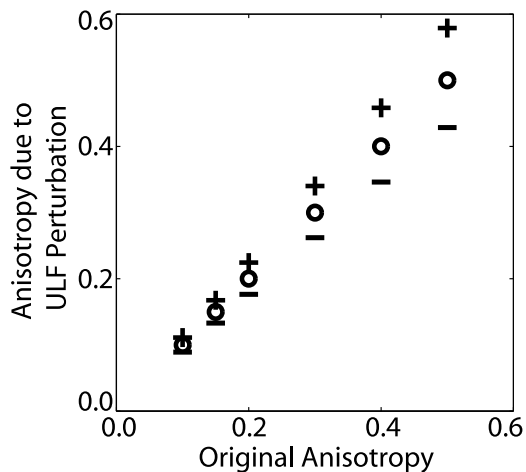
Figure 7. Variation of temperature anisotropy given a magnetic field oscillation of ±10%.

15 keV). In each case, the growth rates for the unperturbed field are compared to the growth rates calculated for the maximum increase in B to $B + 10\%$ (accompanied by an increase in cold number density of 2%, and increases in perpendicular thermal velocity and hot number density given by equations (13) and (14)), and for the maximum decrease in B to $B - 10\%$ (accompanied by the appropriate decreases in hot and cold number density and perpendicular thermal velocity).

[29] The resulting variation in whistler-mode growth rates for the increase in B (+) and the decrease in B (−) are shown in Figure 5a for $A = 0.15$ and $T_{\parallel,e} = 1.5$ keV; Figure 5b for $A = 0.5$ and $T_{\parallel,e} = 1.5$ keV; Figure 5c for $A = 0.15$ and $T_{\parallel,e} = 15$ keV; and Figure 5d for $A = 0.5$ and $T_{\parallel,e} = 15$ keV. In the line plots in each panel, black lines indicate the unperturbed solutions, magenta lines indicate the solutions for $B + 10\%$ and blue lines indicate the solutions for $B - 10\%$. In contrast to Figures 1 and 2, the contour plots in each panel have a linear scale, whereas the line plots employ a logarithmic scale. Interestingly, for all values of initial temperature anisotropy and electron temperature, the variation of unstable frequencies and wavenormal angles given a ±10% variation in ambient magnetic field strength is minimal. The variation in magnitude of the maximum growth rate is largest in Figures 5b and 5d, where the temperature anisotropy is larger ($A = 0.5$). There appears to be no change in the magnitude of the maximum growth rate at all in Figure 5c where $A = 0.15$ and $T_{\parallel,e} = 15$ keV.

[30] The variation in maximum growth rate as a function of temperature anisotropy is studied in further detail in Figures 6a and 6b. These figures show the maximum normalized growth rate for the unperturbed field (asterisks) and the perturbed field (triangles) for (Figure 6a) $T_{\parallel,e} = 1.5$ keV and (Figure 6b) $T_{\parallel,e} = 15$ keV. It is easier to see the variation in maximum growth as a percentage of the unperturbed growth rate, this is shown in Figures 6c and 6d. The percentage change in growth tends to be larger for lower temperature plasma than for higher temperature, although the magnitude of the growth rates is much lower. Figures 6c and 6d show a non-monotonic trend as the temperature anisotropy is increased; the change in growth rates decreases

for low values of A, minimizing at $A \sim 0.2$. The percentage change in maximum growth then increases for $A > 0.2$.

7. Discussion

[31] We have used a local warm plasma dispersion relation and the solutions from a global ideal MHD wave model to investigate how whistler-mode growth rates vary with the slow variation of plasma and field parameters due to a global ULF wave oscillation. In our model, we consider the variation of the magnetic field strength, the cold plasma number density, the hot electron number density and the perpendicular thermal velocity. Variations in these quantities can affect the growth rates of whistler-mode waves due to changes in the temperature anisotropy A, the ratio of plasma frequency to gyrofrequency ω_{pe}/Ω_e and the ratio of hot to cold number density ν. The estimated variation in ν is very small, so we focus here on the behavior of A and ω_{pe}/Ω_e due to the ULF wave. Although whistler-mode growth rates increase for increasing A and ω_{pe}/Ω_e, the ULF wave perturbations will increase one of these parameters while decreasing the other. Figure 7 shows the variation in A for a variation of ±10% in the magnetic field strength. The circles indicate the unperturbed value, and the + and − signs correspond to the temperature anisotropy when the field is enhanced and diminished, respectively. An increase in B leads to an increase in $\theta_\perp$ by equation (14), which leads to an increase in A. On the other hand, the increase in Ω_e due to enhanced B is much larger than the increase in ω_{pe} due to the smaller change in n_e (and hence $\sqrt{n_e}$). Our estimates of the relative increases in B and n_e culminate in a decrease in ω_{pe}/Ω_e. For all cases considered, the unperturbed value of ω_{pe}/Ω_e is 3.0; a compression of the magnetic field reduces this value to 2.7 and a rarefaction of the magnetic field increases it to 3.3. As a result, for small values of the temperature anisotropy, the increase in A appears to be balanced by the decrease in ω_{pe}/Ω_e, and there is little variation in the growth rates of the waves. For larger values of initial A, the larger variation in A overcomes the opposite trend in ω_{pe}/Ω_e, and the variation in growth rates becomes more significant.

[32] One of the key new aspects of this work is that we constrain our choice of wave amplitude at $r = 6.6R_E$ using observations of low-frequency oscillations from the GOES East and West satellites. A decade of data reveals that ULF waves at geosynchronous orbit can only change the magnetic field strength by a few percent, and that even those events are very rare. This constraint is important for all models of the modulation of electromagnetic wave growth by low-frequency waves.

[33] The analysis presented here aims to build upon the original C-K model, which by necessity employed many simplifying assumptions in order to investigate the possible modulation of pitch angle diffusion due to enhancements and reductions in whistler-mode wave growth. The C-K model predicts that the change in maximum growth rates $\Delta\omega_i$ can be estimated by

$$\Delta\omega_i = \frac{(\omega_i(t) - \omega_{i,0})}{\omega_{i,0}} = \frac{b}{A}\sin(\omega_{\mathrm{ULF}}t) \qquad (15)$$

where $\omega_{i,0}$ is the unperturbed growth rate and b is the amplitude of the magnetic field oscillation, as a fraction of B

(a)

(b)
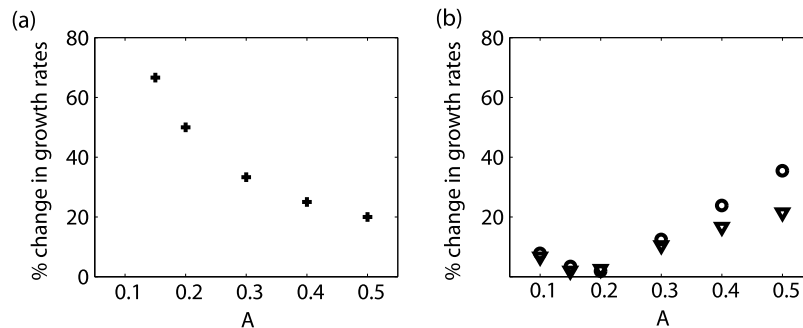
Figure 8. Predicted change in whistler mode growth rates given a magnetic field oscillation of $\pm 10\%$ for the (a) C-K model and (b) the model presented in this paper. Circles indicate solutions with $T_{\parallel,e} = 1.5$ keV and triangles indicate solutions with $T_{\parallel,e} = 15$ keV.

(in this case, $b = 0.1$). For the cases examined in this paper, the change in growth rates predicted by the C-K model should be larger for lower values of the temperature anisotropy. Note that there is no dependence on electron temperature, or electron beta, included in the C-K model. We plot the largest variation predicted by the C-K model in Figure 8a (where $\Delta \omega_i$ is expressed as a percentage) and we reproduce the results from Figures 6c and 6d in Figure 8b as a comparison, where the circles show the results with $T_{\parallel,e} = 1.5$ keV and the triangles show the results with $T_{\parallel,e} = 15$ keV. The C-K model prediction of $\Delta \omega_i$ greatly exceeds our estimates for low values of the temperature anisotropy. The predictions are comparable for the higher values of temperature anisotropy used in this study, but only because each model predicts an opposite trend: the C-K model predicts decreasing $\Delta \omega_i$ with increasing anisotropy, whereas the model presented here predicts an increase in $\Delta \omega_i$ with increasing anisotropy. We should avoid attaching too much significance to this finding, since *Coroniti and Kennel* [1970] warn that the approximations used to obtain equation (15) are crude. However, our analysis raises the interesting possibility that the modulation of growth rates by ULF waves can be quite small, especially for low values of electron anisotropy close to the marginally unstable level [see, e.g., *Gary and Wang*, 1996; *Gary et al.*, 2005; *MacDonald et al.*, 2008]. If the variation in the whistler-mode growth rates is small, then the resulting variation in the pitch angle scattering rates is likely to be small [see *Coroniti and Kennel*, 1970, equation 8]. Our local analysis suggests that the ULF modulation of VLF waves at $r = 6.6 R_E$ near the equator in the magnetosphere is only large enough to significantly alter the pitch angle scattering of electrons when the temperature anisotropy is large, in direct contrast to the predictions of the C-K model.

[34] Note that *Li et al.* [2011] have presented THEMIS observations of whistler-mode wave modulation in compressional waves where the variations in magnetic field strength and number density are exactly out of phase. In this case, the growth rates of the whistler-mode waves are shown to be sufficiently modulated, accounting for the intensifications of whistler-mode activity observed by THEMIS. Interestingly, *Li et al.* [2011] use direct observations to show that in the majority of cases (at $8 < L < 12$), the modulation of the whistler-mode wave growth rates occurs because the ratio of resonant electrons to total electrons is modulated. In some cases at lower L, the whistler-

mode growth rates are modulated because the temperature anisotropy is significantly modulated. The key difference between the plasma number density and magnetic field variations studied by *Li et al.* [2011] and the variations modeled in this paper is that the observations of magnetic field and density perturbations chosen by *Li et al.* [2011] are exactly out of phase, whereas we investigate the case where the number density perturbations are in phase with the magnetic field perturbation. A comparison between this work and that of *Li et al.* [2011] indicates that greater modulation of whistler-mode wave growth rates may be possible when the magnetic field variations, number density variations and hot plasma variations enjoy a specific phase relationship (i.e. exactly out of phase). Constraints of this type may help to explain why not all large-scale ULF wave oscillations are accompanied by pulsations in electron precipitation [*Spanswick et al.*, 2005]. Future models should identify the specific phase relationship between the magnetic field variations and the plasma variations beyond the idealized models used in Sections 4 and 5.

[35] The growth rates shown in Figure 5, calculated using parameters typical of geosynchronous orbit, are essentially field-aligned; the wavenormal angle relative to the local magnetic field ψ is never more than $\sim 15°$. As far as a local treatment is concerned, therefore, a parallel analysis seems appropriate [*Coroniti and Kennel*, 1970; *Sazhin*, 1987; *Summers et al.*, 2009; *Katoh and Omura*, 2007; *Omura et al.*, 2008; *Hikishima et al.*, 2009a, 2009b, 2010]. However, when the magnetospheric propagation of the whistler-mode wave is considered in more detail, it can be shown that the wavenormal angle changes significantly along the raypath [*Huang and Goertz*, 1983; *Huang et al.*, 1983; *Bortnik et al.*, 2006, 2007; *Li et al.*, 2008, 2009]. The full path-integrated gain may therefore be different than calculations of local growth rates suggest. Furthermore, in-situ observations of whistler-mode waves in the magnetosphere indicate that not all whistler-mode waves have parallel wave vectors [*Santolik et al.*, 2009; *Breneman et al.*, 2009]. Ray-tracing calculations [*Li et al.*, 2008, 2009] demonstrate that in a short time (a few seconds), whistler-mode waves can travel through large distances in the magnetosphere. As they travel, they take energy from the surrounding plasma in order to grow, but they do not attain large amplitudes until they are much further along their raypath where the local distribution function may be quite different from where they started. Future analysis of this problem will consider the non-local aspects

of whistler-mode growth and how they might be altered by a slowly oscillating ULF wavefield.

8. Summary and Conclusions

[36] We use a warm plasma dispersion relation to calculate the growth rates for whistler-mode waves for parameters indicative of the equatorial region of the magnetosphere at geosynchronous orbit. A limited parameter study of the variation of whistler-mode growth with temperature anisotropy and ω_{pe}/Ω_e shows that both parameters lead to an increase in whistler-mode growth rates and the range of unstable perpendicular wave numbers. Changes in temperature anisotropy also lead to changes in the range of unstable frequencies. The linear growth rate solutions are used to estimate by how much whistler-mode growth rates vary in the presence of a ULF wave oscillation at geosynchronous orbit. We use a statistical survey of GOES East and West data over nearly a decade to determine the possible magnitude of changes to the magnetic field strength due to compressional ULF waves at geosynchronous orbit. The distribution of wave amplitudes convincingly shows that, at most, the magnetic field strength changes by only a few percent. An ideal MHD simulation of global ULF wave oscillations is used to estimate the accompanying change in cold plasma number density. We estimate the effect of the ULF magnetic field strength variation on the number density and average perpendicular energy of the hot electron component, and use these estimates to simulate the action of a long period ULF wave oscillation on the solutions of the warm plasma dispersion relation. Our calculations show that the range of unstable frequencies and wavenormal angles remains relatively constant during the ULF modulation, but that the maximum growth rates of the waves are modulated. This modulation is only significant for large values of the electron temperature anisotropy; at lower values of the temperature anisotropy, the balance between increases in temperature anisotropy and decreases in ω_{pe}/Ω_e results in a very small variation in growth rates, even for an extreme oscillation of ±10% of the ambient magnetic field. Our local treatment of the variation in whistler-mode growth rates suggests that even substantial ULF waves can only provide sufficient changes in the local whistler-mode wave growth rates when the temperature anisotropy is large.

Appendix A

[37] *Summers et al.* [1994] present expressions for the elements of the dielectric tensor K_{ij} for bi-Lorentzian distribution functions (see equation (7)). We assume that both electrons and protons can be described by a majority cold population and a tenuous warm component where $\nu \ll 1$ is the fraction of warm to cold plasma number density (for simplicity we assume this fraction is the same for electrons and protons),

$$\begin{bmatrix} K_{xx} - 1 \\ K_{xy} \\ K_{yy} - 1 \end{bmatrix} = \sum_\alpha \frac{\nu \omega_{p\alpha}^2}{\omega^2 \lambda_\alpha^2} \sum_{n=-\infty}^{\infty} \begin{bmatrix} n^2 \\ in \\ 1 \end{bmatrix} \left\{ A_\alpha \begin{bmatrix} S_1 \\ S_3 \\ S_5 \end{bmatrix} \right.$$
$$\left. + \left(A_\alpha \xi_{n\alpha} + \frac{\omega}{k_\| \theta_{\|,\alpha}} \right) \begin{bmatrix} S_2 \\ S_4 \\ S_6 \end{bmatrix} \right\}, \quad (A1)$$

$$\begin{bmatrix} K_{xz} \\ K_{yz} \\ K_{zz} - 1 \end{bmatrix} = \sum_\alpha \frac{\nu \omega_{p\alpha}^2}{\omega^2} \frac{\theta_{\|\alpha}^2}{\theta_{\perp\alpha}^2} \sum_{n=-\infty}^{\infty} \left(A_\alpha \xi_{n\alpha} + \frac{\omega}{k_\| \theta_{\|,\alpha}} \right)$$
$$\cdot \begin{bmatrix} \sqrt{2}n/\lambda_\alpha^{3/2} \\ -\sqrt{2}i/\lambda_\alpha^{3/2} \\ 2(\theta_{\|\alpha}/\theta_{\perp\alpha})(\xi_{n\alpha}/\lambda_\alpha) \end{bmatrix} \left\{ \begin{bmatrix} S_1 \\ S_3 \\ S_1 \end{bmatrix} + \xi_{n\alpha} \begin{bmatrix} S_2 \\ S_4 \\ S_2 \end{bmatrix} \right\}. \quad (A2)$$

Above, each plasma species α has charge q_α, mass m_α and cold number density n_α. $\Omega_\alpha = q_\alpha B_0/m_\alpha$ is the gyrofrequency and $\omega_{p\alpha} = (m_\alpha q_\alpha^2/(\epsilon_0 m_\alpha))^{1/2}$ is the plasma frequency, $\lambda_\alpha = (1/2)(k_\perp \theta_{\perp\alpha}/\Omega_\alpha)^2$, and $\xi_{n\alpha} = (\omega - n\Omega_\alpha)/(k_\| \theta_{\|\alpha})$.

[38] The S_i can be evaluated using the following expressions,

$$S_1 = 2\lambda_\alpha \sigma_{odd} \int_0^1 \frac{(1/y - 1)J_n^2(r/y - r)}{y^2 \left(\kappa + 1 - \frac{2}{y} + \frac{1}{y^2} \right)^{\kappa+3/2}} dy, \quad (A3)$$

$$S_2 = 2\lambda_\alpha \sigma_{even} \int_0^1 \frac{(1/y - 1)J_n^2(r/y - r)}{y^2 \left(\kappa + 1 - \frac{2}{y} + \frac{1}{y^2} \right)^{\kappa+2}}$$
$$\cdot Z_{\kappa+1}^\star \left[\left(\frac{\kappa + 1}{\left(\kappa + 1 - \frac{2}{y} + \frac{1}{y^2} \right)} \right)^{1/2} \xi_{n\alpha} \right] dy, \quad (A4)$$

$$S_3 = (2\lambda_\alpha)^{3/2} \sigma_{odd} \int_0^1 \frac{(1/y - 1)^2 J_n(r/y - r)J_n'(r/y - r)}{y^2 \left(\kappa + 1 - \frac{2}{y} + \frac{1}{y^2} \right)^{\kappa+3/2}} dy, \quad (A5)$$

$$S_4 = (2\lambda_\alpha)^{3/2} \sigma_{even} \int_0^1 \frac{(1/y - 1)^2 J_n(r/y - r)J_n'(r/y - r)}{y^2 \left(\kappa + 1 - \frac{2}{y} + \frac{1}{y^2} \right)^{\kappa+2}}$$
$$\cdot Z_{\kappa+1}^\star \left[\left(\frac{\kappa + 1}{\left(\kappa + 1 - \frac{2}{y} + \frac{1}{y^2} \right)} \right)^{1/2} \xi_{n\alpha} \right] dy, \quad (A6)$$

$$S_5 = 4\lambda_\alpha^2 \sigma_{odd} \int_0^1 \frac{(1/y - 1)^3 \{J_n'(r/y - r)\}^2}{y^2 \left(\kappa + 1 - \frac{2}{y} + \frac{1}{y^2} \right)^{\kappa+3/2}} dy, \quad (A7)$$

$$S_6 = 4\lambda_\alpha^2 \sigma_{even} \int_0^1 \frac{\left(\frac{1}{y} - 1 \right)^3 \{J_n'\left(\frac{r}{y} - r \right)\}^2}{y^2 \left(\kappa + 1 - \frac{2}{y} + \frac{1}{y^2} \right)^{\kappa+2}}$$
$$\cdot Z_{\kappa+1}^\star \left[\left(\frac{\kappa + 1}{\kappa + 1 - \frac{2}{y} + \frac{1}{y^2}} \right)^{1/2} \xi_{n\alpha} \right] dy. \quad (A8)$$

where $r = \sqrt{2\lambda_\alpha}$, $\sigma_{odd} = (\kappa + \frac{1}{2})(\kappa - \frac{1}{2})\kappa^{\kappa-1/2}$, $\sigma_{even} = (\kappa + 1/\kappa)^{3/2}(\kappa - \frac{1}{2})\kappa^{\kappa+1}$, the $J_n(x)$ are Bessel functions of the first kind with argument x, and $Z_{\kappa+1}^*$ is the modified plasma dispersion function introduced by *Summers and Thorne* [1991].

[39] In work by *Summers et al.* [1994], the S_i are first written as integrals over the variable $\mu = k_\perp v_\perp / \Omega_\alpha$, which runs from 0 to ∞. In order to treat the limit $k_\perp \rightarrow 0$ (i.e. parallel propagation), they advise the substitution $\phi = \mu/(2\lambda_\alpha)^{1/2}$, however, the limits of integration remain 0 and ∞. So that we may efficiently evaluate the integrals of the S_i numerically, we have performed a further change of variables $y = 1/(1 + \phi)$, to obtain a definite integral with limits 0 and 1. There is still the problem that the integrands are undefined at the limit $y = 0$, however this problem can be satisfactorily dealt with numerically [see, e.g., *Press et al.*, 2007].

[41] Robert Lysak thanks the reviewers for their assistance in evaluating this paper.

References

Anderson, R. R., and K. Maeda (1977), VLF emissions associated with enhanced magnetospheric electrons, *J. Geophys. Res.*, *82*(1), 135–146.

Anger, C. D., R. R. Brown, D. S. Evans, and J. R. Barcus (1963), Long-period pulsations in electron precipitation associated with hydromagnetic waves in auroral zone, *J. Geophys. Res.*, *68*(10), 3306–3310.

Arthur, C. W., J. Bjordal, and T. J. Rosenberg (1979), Pc3 magnetic pulsations and precipitation of energetic electrons, *J. Geophys. Res.*, *84*(A8), 4125–4133.

Asnes, A., J. Stadsnes, J. Bjordal, N. Ostgaard, D. L. Detrick, T. J. Rosenberg, and S. E. Haaland (2004), Pi2-pulsations observed in energetic electron precipitation and magnetic field in association with a substorm surge, *Ann. Geophys.*, *22*(6), 2097–2105.

Berkey, F. T. (1974), Coruscation of auroral particle flux at College-Alaska, *J. Atmos. Terr. Phys.*, *36*(5), 881–887.

Bortnik, J., U. S. Inan, and T. F. Bell (2006), Landau damping and resultant unidirectional propagation of chorus waves, *Geophys. Res. Lett.*, *33*, L03102, doi:10.1029/2005GL024553.

Bortnik, J., R. M. Thorne, N. P. Meredith, and O. Santolik (2007), Ray tracing of penetrating chorus and its implications for the radiation belts, *Geophys. Res. Lett.*, *34*, L15109, doi:10.1029/2007GL030040.

Breneman, A. W., C. A. Kletzing, J. Pickett, J. Chum, and O. Santolik (2009), Statistics of multispacecraft observations of chorus dispersion and source location, *J. Geophys. Res.*, *114*, A06202, doi:10.1029/2008JA013549.

Brinca, A. L. (1972), Stability of obliquely propagating whistlers, *J. Geophys. Res.*, *77*(19), 3495–3507.

Brown, R. R. (1964), Study of slowly varying and pulsating ionospheric absorption events in auroral zone, *J. Geophys. Res.*, *69*(11), 2315–2321.

Brown, R. R. (1975), Further studies of long-period pulsations in ionospheric absorption at auroral zone latitudes, *J. Geophys. Res.*, *80*(7), 1023–1025.

Christon, S. P., D. G. Mitchell, D. J. Williams, L. A. Frank, C. Y. Huang, and T. E. Eastman (1988), Energy-spectra of plasma sheet ions and electrons from approximately 50 eV/e to approximately 1 MeV during plasma temperature transitions, *J. Geophys. Res.*, *93*(A4), 2562–2572.

Coroniti, F. V., and C. F. Kennel (1970), Electron precipitation pulsations, *J. Geophys. Res.*, *75*(7), 1279–1289.

Denton, M. H., M. F. Thomsen, H. Korth, S. Lynch, J. C. Zhang, and M. W. Liemohn (2005), Bulk plasma properties at geosynchronous orbit, *J. Geophys. Res.*, *110*, A07223, doi:10.1029/2004JA010861.

Degeling, A. W., L. G. Ozeke, R. Rankin, I. R. Mann, and K. Kabin (2008), Drift resonant generation of peaked relativistic electron distributions by Pc 5 ULF waves, *J. Geophys. Res.*, *113*, A02208, doi:10.1029/2007JA012411.

Gary, S. P. (1993), *Theory of Space Plasma Microinstabilities*, 181 pp., Cambridge Univ. Press, Cambridge, U. K.

Gary, S. P., and J. Wang (1996), Whistler instability: Electron anisotropy upper bound, *J. Geophys. Res.*, *101*(A5), 10,749–10,754.

Gary, S. P., B. Lavraud, M. F. Thomsen, B. Lefebvre, and S. J. Schwartz (2005), Electron anisotropy constraint in the magnetosheath: Cluster observations, *Geophys. Res. Lett.*, *32*, L13109, doi:10.1029/2005GL023234.

Glassmeier, K. H., W. Baumjohann, A. Korth, and P. Gough (1988), High-latitude Pi2 pulsations, ELF intensity, and particle-flux variations—A case-study, *Ann. Geophys.*, *6*(3), 287–295.

Hargreaves, J. K. (1969), Auroral absorption of HF radio waves in ionosphere—A review of results from first decade of riometry, *Proc. IEEE*, *57*(8), 1348–1373.

Heacock, R. R., and R. D. Hunsucker (1977), Study of concurrent magnetic-field and particle precipitation pulsations, 0.005 to 0.5 Hz, recorded near College, Alaska, *J. Atmos. Terr. Phys.*, *39*(4), 487–501.

Hellberg, M. A., and R. L. Mace (2002), Generalized plasma dispersion function for a plasma with a kappa-Maxwellian velocity distribution, *Phys. Plasmas*, *9*(5), 1495–1504.

Hikishima, M., S. Yagitani, Y. Omura, and I. Nagano (2009a), Full particle simulation of whistler-mode rising chorus emissions in the magnetosphere, *J. Geophys. Res.*, *114*, A01203, doi:10.1029/2008JA013625.

Hikishima, M., S. Yagitani, Y. Omura, and I. Nagano (2009b), Coherent nonlinear scattering of energetic electrons in the process of whistler-mode chorus generation, *J. Geophys. Res.*, *114*, A10205, doi:10.1029/2009JA014371.

Hikishima, M., Y. Omura, and D. Summers (2010), Microburst precipitation of energetic electrons associated with chorus wave generation, *Geophys. Res. Lett.*, *37*, L07103, doi:10.1029/2010GL042678.

Huang, C. L., H. E. Spence, H. J. Singer, and W. J. Hughes (2010), Modeling radiation belt radial diffusion in ULF wave fields: 1. Quantifying ULF wave power at geosynchronous orbit in observations and in global MHD model, *J. Geophys. Res.*, *115*, A06215, doi:10.1029/2009JA014917.

Huang, C. Y., and C. K. Goertz (1983), Ray-tracing studies and path-integrated gains of ELF unducted whistler-mode waves in the Earth's magnetosphere, *J. Geophys. Res.*, *88*(A8), 6181–6187.

Huang, C. Y., C. K. Goertz, and R. R. Anderson (1983), A theoretical-study of plasmaspheric hiss generation, *J. Geophys. Res.*, *88*(A10), 7927–7940.

Hunsucker, R. D., H. F. Bates, and A. E. Belon (1972), Observations of simultaneous auroral D and E layers with incoherent scatter radar, *Nat. Phys. Sci.*, *239*(94), 102–104.

Katoh, Y., and Y. Omura (2007), Computer simulation of chorus wave generation in the Earth's inner magnetosphere, *Geophys. Res. Lett.*, *34*, L03102, doi:10.1029/2006GL028594.

Katoh, Y., and Y. Omura (2011), Amplitude dependence of frequency sweep rates of whistler-mode chorus emissions, *J. Geophys. Res.*, *116*, A07201, doi:10.1029/2011JA016496.

Kennel, C. F., and H. E. Petschek (1966), Limit on stably trapped particle fluxes, *J. Geophys. Res.*, *71*(1), 1–28.

Kletzing, C. A., J. D. Scudder, E. E. Dors, and C. Curto (2003), Auroral source region: Plasma properties of the high-latitude plasma sheet, *J. Geophys. Res.*, *108*(A10), 1360, doi:10.1029/2002JA009678.

Li, W., R. M. Thorne, N. P. Meredith, R. B. Horne, J. Bortnik, Y. Y. Shprits, and B. Ni (2008), Evaluation of whistler-mode chorus amplification during an injection event observed on CRRES, *J. Geophys. Res.*, *113*, A09210, doi:10.1029/2008JA013129.

Li, W., et al. (2009), Evaluation of whistler-mode chorus intensification on the nightside during an injection event observed on the THEMIS spacecraft, *J. Geophys. Res.*, *114*, A00C14, doi:10.1029/2008JA013554.

Li, W., R. M. Thorne, J. Bortnik, Y. Nishimura, and V. Angelopoulos (2011), Modulation of whistler-mode chorus waves: 1. Role of compressional Pc4–5 pulsations, *J. Geophys. Res.*, *116*, A06205, doi:10.1029/2010JA016312.

MacDonald, E. A., M. H. Denton, M. F. Thomsen, and S. P. Gary (2008), Superposed epoch analysis of a whistler instability criterion at geosynchronous orbit during geomagnetic storms, *J. Atmos. Sol. Terr. Phys.*, *70*(14), 1789–1796.

Mace, R. L., and M. A. Hellberg (2009), A new formulation and simplified derivation of the dispersion function for a plasma with a kappa velocity distribution, *Phys. Plasmas*, *16*(7), 072113.

Mace, R. L., and R. D. Sydora (2010), Parallel whistler instability in a plasma with an anisotropic bi-kappa distribution, *J. Geophys. Res.*, *115*, A07206, doi:10.1029/2009JA015064.

Manninen, J., N. G. Kleimenova, O. V. Kozyreva, and T. Turunen (2010), Pc5 geomagnetic pulsations, pulsating particle precipitation, and VLF chorus: Case study on 24 November 2006, *J. Geophys. Res.*, *115*, A00F14, doi:10.1029/2009JA014837.

McPherron, R. L., G. K. Parks, F. V. Coroniti, and S. H. Ward (1968), Studies of magnetospheric substorm: 2. Correlated magnetic micropulsations and electron precipitation occurring during auroral substorms, *J. Geophys. Res.*, *73*(5), 1697–1713.

Morrison, K. (1990), Quasi-periodic VLF emissions and concurrent magnetic pulsations seen at L = 4, *Planet. Space Sci.*, *38*, 1555–1565.

Olson, J. V., G. Rostoker, and G. Olchowy (1980), A study of concurrent riometer and magnetometer variations in the Pc 4–5 pulsation band, *J. Geophys. Res.*, *85*(A4), 1695–1702.

Omholt, A. (1971), *The Optical Aurora*, Springer, Berlin.

Omura, Y., Y. Katoh, and D. Summers (2008), Theory and simulation of the generation of whistler-mode chorus, *J. Geophys. Res.*, *113*, A04223, doi:10.1029/2007JA012622.

Omura, Y., M. Hikishima, Y. Katoh, D. Summers, and S. Yagitani (2009), Nonlinear mechanisms of lower-band and upper-band VLF chorus emissions in the magnetosphere, *J. Geophys. Res.*, *114*, A07217, doi:10.1029/2009JA014206.

Paquette, J. A., D. L. Matthews, T. J. Rosenberg, L. J. Lanzerotti, and U. S. Inan (1994), Source regions of long-period pulsation events in electron-precipitation and magnetic-fields at South Pole station, *J. Geophys. Res.*, *99*(A3), 3869–3877.

Parthasarathy, R., and V. P. Hessler (1964), Periodic covariation of radio-wave absorption, Earth currents and other associated phenomena in auroral zone, *J. Geophys. Res.*, *69*(13), 2867–2871.

Posch, J. L., M. J. Engebretson, A. T. Weatherwax, D. L. Detrick, W. J. Hughes, and C. G. Maclennan (1999), Characteristics of broadband ULF magnetic pulsations at conjugate cusp latitude stations, *J. Geophys. Res.*, *104*(A1), 311–331.

Press, W. H., S. A. Teukolsky, W. T. Vetterling, and B. P. Flannery (2007), *Numerical Recipes: The Art of Scientific Computing*, Cambridge Univ. Press, Cambridge, U. K.

Rae, I. J., I. R. Mann, Z. C. Dent, D. K. Milling, E. F. Donovan, and E. Spanswick (2007), Multiple field line resonances: Optical, magnetic and absorption signatures, *Planet. Space Sci.*, *55*, 701–713.

Roldugin, V. C., and A. V. Roldugin (2008), Pc5 pulsations on the ground, in the magnetosphere, and in the electron precipitation: Event of 19 January 2005, *J. Geophys. Res.*, *113*, A04222, doi:10.1029/2007JA012553.

Santolik, O., D. A. Gurnett, J. S. Pickett, J. Chum, and N. Cornilleau-Wehrlin (2009), Oblique propagation of whistler-mode waves in the chorus source region, *J. Geophys. Res.*, *114*, A00F03, doi:10.1029/2009JA014586.

Sauer, K., and R. D. Sydora (2010), Beam-excited whistler waves at oblique propagation with relation to stereo radiation belt observations, *Ann. Geophys.*, *28*(6), 1317–1325.

Sazhin, S. S. (1987), An analytical model of quasi-periodic ELF-VLF emissions, *Planet. Space Sci.*, *35*, 1267–1274.

Sazhin, S. S. (1991), Landau damping of low-frequency whistler-mode waves, *Ann. Geophys.*, *9*(10), 690–695.

Singer, H. J., L. Matheson, R. Grubb, A. Newman, and S. D. Bouwer (1996), Monitoring space weather with the GOES magnetometers, *SPIE Conf. Proc.*, *2812*, 299–308.

Singh, R. P., R. P. Patel, K. Singh, and A. K. Singh (2005), Observation of pulsing hiss at low latitudes, *J. Atmos. Sol. Terr. Phys.*, *67*(16), 1497–1503.

Smith, A. J., M. J. Engebretson, E. M. Klatt, U. S. Inan, R. L. Arnoldy, and H. Fukunishi (1998), Periodic and quasiperiodic ELF/VLF emissions observed by an array of Antarctic stations, *J. Geophys. Res.*, *103*(A10), 23,611–23,622.

Spanswick, E., E. Donovan, and G. Baker (2005), Pc5 modulation of high energy electron precipitation: Particle interaction regions and scattering efficiency, *Ann. Geophys.*, *23*(5), 1533–1542.

Stix, T. H. (1992), *Waves in Plasmas*, 566 pp., Am. Inst. of Phys., New York.

Summers, D., and R. M. Thorne (1991), The modified plasma dispersion function, *Phys. Fluids B*, *3*(8), 1835–1847.

Summers, D., S. Xue, and R. M. Thorne (1994), Calculation of the dielectric tensor for a generalized Lorentzian (kappa) distribution function, *Phys. Plasmas*, *1*(6), 2012–2025.

Summers, D., R. M. Thorne, and H. Matsumoto (1996), Evaluation of the modified plasma dispersion function for half-integral indices, *Phys. Plasmas*, *3*(7), 2496–2501.

Summers, D., R. Tang, and R. M. Thorne (2009), Limit on stably trapped particle fluxes in planetary magnetospheres, *J. Geophys. Res.*, *114*, A10210, doi:10.1029/2009JA014428.

Tsurutani, B. T., and E. J. Smith (1974), Postmidnight chorus—Substorm phenomenon, *J. Geophys. Res.*, *79*(1), 118–127.

Ullaland, S. L., H. Trefall, G. Kremser, and A. Bewersdorff (1967), Observations of large-scale coherent pulsating electron precipitation events in auroral zone accompanied by geomagnetic continuous pulsations, *J. Atmos. Terr. Phys.*, *29*(4), 395–410.

Xiao, F. L., and X. Feng (2006), Modelling density and anisotropy of energetic electrons along magnetic field lines, *Plasma Sci. Technol.*, *8*(3), 279–284.

Xiao, F. L., R. M. Thorne, and D. Summers (1998), Instability of electromagnetic R-mode waves in a relativistic plasma, *Phys. Plasmas*, *5*(7), 2489–2497.

Yuan, F. F. F., and F. Jacka (1969), Simultaneous geomagnetic and cosmic noise absorption pulsations near geomagnetic noon, *Nature*, *222*(5194), 653–654.

Ziauddin, S. (1960), Simultaneous observations of pulsations in the geomagnetic field and in ionospheric absorption, *Can. J. Phys.*, *38*(12), 1714–1715.

A. W. Degeling, K. R. Murphy, I. J. Rae, R. Rankin, and C. E. J. Watt, Department of Physics, University of Alberta, Edmonton, AB T6G 2G7, Canada. (degeling@ualberta.ca; kmurphy@ualberta.ca; jonathan.rae@ualberta.ca; rrankin@ualberta.ca; watt@ualberta.ca)

H. J. Singer, NOAA Space Environment Center, 325 Broadway, Boulder, CO 80305, USA. (howard.singer@noaa.gov)